Gravitational waves from equatorially eccentric extreme mass ratio inspirals around swirling-Kerr black holes*

Yuhang Gu (顾雨杭)[1] Songbai Chen (陈松柏)[1,2†] Jiliang Jing (荆继良)[1,2‡]

[1]Department of Physics, Institute of Interdisciplinary Studies, Hunan Research Center of the Basic Discipline for Quantum Effects and Quantum Technologies, Key Laboratory of Low Dimensional Quantum Structures and Quantum Control of Ministry of Education, Synergetic Innovation Center for Quantum Effects and Applications, Hunan Normal University, Hunan 410081, China
[2]Center for Gravitation and Cosmology, College of Physical Science and Technology, Yangzhou University, Yangzhou 225009, China

Abstract: The swirling-Kerr black hole is a novel solution of vacuum general relativity and has an extra swirling parameter characterizing the rotation of spacetime background. We study the gravitational waves generated by extreme mass ratio inspirals (EMRIs) along eccentric orbits on the equatorial plane in this novel swirling spacetime. Our findings indicate that this swirling parameter leads to a delayed phase shift in the gravitational waveforms. Furthermore, we investigate the effects of the swirling parameter on the potential issue of waveform confusion caused by the orbital eccentricity and semi-latus rectum parameters. As the swirling parameter increases, the relative variations in the eccentricity increase, whereas the variations in the semi-latus rectum rapidly decrease. The trends related to changes in the orbital eccentricity and semi-latus rectum with the swirling parameter resemble those observed with the MOG parameter in Scalar-Tensor-Vector-Gravity (STVG) theory but with different rates of change. Furthermore, our results also reveal that the effects of the background swirling parameter on the relative variations in the eccentricity and semi-latus rectum are distinct from those of the black hole spin parameter. These results provide deeper insights into the properties of EMRI gravitational waves and background swirling.

Keywords: gravitational waves, extreme mass ratio inspirals, black hole, swirling

DOI: 10.1088/1674-1137/ae1afc **CSTR:** 32044.14.ChinesePhysicsC.50025107

I. INTRODUCTION

Gravitational wave astrophysics has entered a new era with the direct detection of hundreds of gravitational wave events [1−3]. Among various sources of gravitational waves, extreme mass ratio inspiral (EMRI) systems [4−19] are of particular interest for future space-based gravitational wave detectors [20−26] because their gravitational waves are in the lower frequency band [27−31], making them difficult to explore using the current ground-based detectors. In an EMRI system, a stellar-mass object (the secondary with mass μ) slowly spirals inward toward the central supermassive black hole (the primary with mass M) owing to gravitational emission and undergoes numerous orbits before ultimately plunging in. During this evolution, the gravitational waveforms generated by EMRIs are closely related to the trajectory of the smaller object, which imprints characteristic information on the spacetime geometry around the supermassive black hole. This means that EMRI gravitational waves are invaluable probes to study the properties of supermassive black holes and examine gravitational theories. EMRI gravitational waves have been extensively applied to constrain the nature of Kerr spacetime [32−44] and test theories of gravity, including Einstein's general relativity, Brans-Dicke theory [45−47], dynamical Chern-Simons gravity [48−50], quantum gravity [51−53], and Einstein-Cartan theory [54−59]. Recently, EMRI gravitational waves have also served as a power tool to detect dark matter around supermassive black holes [60−62] and probe scalar charges induced by dipole radiation [63−72]. EMRI gravitational waves can be used as standard sirens to investigate the expansion history of the universe and further constrain cosmological parameters [73].

The Kerr black hole is an important vacuum solution of stationary and axisymmetric black holes in general relativity. Therefore, it is important to study gravitational waves in rotating vacuum black hole spacetimes, which deviate from their typical Kerr counterparts, because this

Received 5 September 2025; Accepted 3 November 2025; Accepted manuscript online 4 November 2025

* Supported by the National Natural Science Foundation of China (12275078, 11875026, 12035005, 2020YFC2201400) and the innovative research group of Hunan Province (2024JJ1006)

† E-mail: csb3752@hunnu.edu.cn
‡ E-mail: jljing@hunnu.edu.cn

would provide extra information on spacetime and gravity. Recently, another interesting and rotating vacuum solution of the Einstein field equations was obtained by Astorino et al. [74], by exploiting the Ernst formalism [75, 76] in combination with the Ehlers transformation, starting from a Kerr seed spacetime. This black hole is characterized by three parameters: the black hole mass and spin parameters and the swirling parameter. The swirling parameter describes the background's rotation, which can be interpreted as a gravitational whirlpool. The spin-spin interaction between the black hole and background frame dragging results in the breaking of the symmetry of spacetime geometry owing to an additional force acting on the axis. The swirling-Kerr black hole co-rotates with the swirling background in one hemisphere and counter-rotates in the other because the black hole spin does not affect its sign with respect to the equatorial plane. The breaking of symmetry leads to non-removable conical singularities along the symmetry axis; therefore, there is a cosmic string or strut to compensate for the force effect induced by the spin-spin interaction. The swirling-Kerr black hole solution possesses two horizon surfaces located at $r_\pm = M \pm \sqrt{M^2 - a^2}$, which is independent of the swirling parameter and equivalent to that of the Kerr case. However, background swirling deforms the horizon geometry [74]. In this swirling-Kerr black hole spacetime, there are no closed time-like curves; hence, it is less exotic than the Gödel or Taub-NUT spacetime [74]. The geodesic in the swirling universe is no longer decoupled because the spacetime is no longer of Petrov type D, which can yield chaotic particle motion in this spacetime [77, 78]. Moreover, the swirling parameter drives the light rings outside the equatorial plane, which results in the contour of the shadow taking on a tilted oblate shape [79]. Recent studies analyzed the geometrically thick equilibrium tori orbiting a Schwarzschild black hole with the swirling parameter [80] and a swirling-Kerr black hole [81] and explored the new effects arising from background swirling on the equilibrium tori around the black holes. Studies on swirling black holes have been generalized to the electromagnetic case [82, 83]. These studies shed new light on black holes with background swirling.

The main objectives of this study are to investigate the gravitational waves originating from equatorially eccentric EMRIs around a swirling-Kerr black hole, probe the new effects arising from background swirling, and understand how they differ from those of a Kerr black hole. For EMRIs, direct numerical relativity simulations are computationally prohibitive owing to the vast separation of timescales and spatial scales. The numerical kludge (NK) approach addresses this by hybridizing multiple approximate theories to generate sufficiently accurate gravitational waveform templates at a fraction of the computational cost. Therefore, we employ the NK scheme [84, 85] to simulate gravitational waveforms generated by the EMRI system and discuss how background swirling influences these waveforms. We also analyze the gravitational waveform confusion problem.

This paper is organized as follows. In Sec. II, we briefly review the swirling-Kerr black hole solution [74] and equatorial EMRI systems. In Sec. III, we present the properties of EMRI gravitational waves in the swirling background and analyze the effects of the swirling and black hole spin parameters. Finally, in Sec. IV, we present a summary.

II. EQUATORIAL EMRI SYSTEM WITHIN THE FRAMEWORK OF SWIRLING KERR SPACETIMES

First, let us briefly review the Kerr black hole solution embedded in a rotating background. It is a stationary, axially symmetric, and non-asymptotically flat black hole solution of the vacuum Einstein equations, which can be obtained through an Ehlers transformation on the Kerr solution seed [74]. A swirling Kerr black hole possesses the swirling and spin parameters, and its metric form in the Boyer-Lindquist coordinates can be written as

$$\mathrm{d}s^2 = F(\mathrm{d}\phi - \omega \mathrm{d}t)^2 + F^{-1}\left[-\rho^2\mathrm{d}t^2 + \Sigma\sin^2\theta\left(\frac{\mathrm{d}r^2}{\Delta} + \mathrm{d}\theta^2\right)\right], \tag{1}$$

where functions F and ω can be expressed as a finite power series of the swirling parameter j,

$$F^{-1} = \chi_{(0)} + j\chi_{(1)} + j^2\chi_{(2)}, \quad \omega = \omega_{(0)} + j\omega_{(1)} + j^2\omega_{(2)}. \tag{2}$$

The expansion coefficients $\chi_{(i)}$ and $\omega_{(i)}$ are

$$\begin{aligned}\chi_{(0)} &= \frac{R^2}{\Sigma\sin^2\theta},\\ \chi_{(1)} &= \frac{4aM\Xi\cos\theta}{\Sigma\sin^2\theta},\\ \chi_{(2)} &= \frac{4a^2M^2\Xi^2\cos^2\theta + \Sigma^2\sin^4\theta}{R^2\Sigma\sin^2\theta},\end{aligned} \tag{3}$$

and

$$\omega_{(0)} = \frac{2aMr}{-\Sigma}, \qquad \omega_{(1)} = \frac{4\cos\theta[-a\Omega(r-M)+Ma^4-r^4(r-2M)-\Delta a^2 r]}{-\Sigma},$$
$$\omega_{(2)} = -\frac{2M\{3ar^5-a^5(r+2M)+2a^3r^2(r+3M)-r^3(\cos^2\theta-6)\Omega+a^2[\cos^2\theta(3r-2M)-6(r-M)]\Omega\}}{\Sigma}, \tag{4}$$

where

$$\Delta = r^2-2Mr+a^2, \qquad \rho^2 = \Delta\sin^2\theta,$$
$$\Sigma = (r^2+a^2)^2-\Delta a^2\sin^2\theta, \qquad \Omega = \Delta a\cos^2\theta,$$
$$R^2 = r^2+a^2\cos^2\theta, \qquad \Xi = r^2(\cos^2\theta-3)-a^2(1+\cos^2\theta). \tag{5}$$

Here, M and a denote the mass parameter of the black hole and the angular momentum per unit mass, respectively. It reduces to a pure Kerr black hole when the swirling parameter $j=0$ and to a Schwarzschild black hole in swirling universes when the black hole spin $a=0$. The spin-spin interaction between the black hole and background dragging leads to a conical singularity along the symmetry axes [74], which deforms the horizon geometry and enhances symmetry breaking with respect to the spacetime properties. The presence of j indicates that the northern and southern hemispheres of the swirling Kerr black hole rotate in opposite directions, which differs from the pure Kerr black hole case.

In the swirling Kerr black hole spacetime, the Lagrangian of a timelike particle moving along the geodesic is

$$\mathcal{L} = \frac{1}{2}g_{\mu\nu}\dot{x}^\mu\dot{x}^\nu. \tag{6}$$

This Lagrangian is independent of the coordinates t and ϕ, which means that there are two conserved quantities for the motion of the timelike particle along the geodesics:

$$E = -u_t = -g_{tt}u^t - g_{t\phi}u^\phi, \qquad L_z = u_\phi = g_{t\phi}u^t + g_{\phi\phi}u^\phi, \tag{7}$$

where

$$u^t = \frac{F(E+L_z\omega)}{\rho^2}, \qquad u^\phi = \frac{L_z}{F} - \frac{F\omega(E+L_z\omega)}{\rho^2}. \tag{8}$$

Here, E and L_z correspond to the energy and angular momentum of a particle, respectively. The timelike condition $g_{\mu\nu}u^\mu u^\nu = -1$ leads to a constraint condition for the particle's motion:

$$h = g_{tt}\dot{t}^2 + g_{rr}\dot{r}^2 + g_{\theta\theta}\dot{\theta}^2 + g_{\varphi\varphi}\dot{\varphi}^2 + 2g_{t\varphi}\dot{t}\dot{\varphi} + 1 = 0. \tag{9}$$

Generally, this first-order differential equation is non-separable, and there is no Carter constant Q for the particle's motion. Therefore, we consider only the case in which the particle's geodesics are limited in the equatorial plane and probe the corresponding effects of the swirling parameter on gravitational waves from EMRIs.

For a bounded Kepler geodesic in the equatorial plane, the orbit can be characterized by the eccentricity e and semi-major axis p with the forms

$$e = \frac{r_a - r_p}{r_a + r_p}, \qquad p = \frac{2r_a r_p}{r_a + r_p}. \tag{10}$$

Here, r_a and r_p represent the apastron and periastron in the geodesic orbit, respectively. For the equatorial orbits, the eccentricity e and semi-major axis p can be determined based on the particle's E and L_z. To circumvent the numerical difficulties frequently associated with turning points, we can transition the integration variable r to the angular coordinate χ [84, 85]:

$$r = \frac{p}{1+e\cos\chi}. \tag{11}$$

As the parameter χ transforms between 0 and 2π, the coordinate r travels back and forth between the apostolic points r_a and r_p. The effective potential V_r for the geodesics in the equatorial plane is

$$V_r = -1 - \frac{L_z^2}{F} + \frac{F(E+L_z\omega)^2}{\rho^2}. \tag{12}$$

With the conditions $V_r(r_a) = 0$ and $V_r(r_p) = 0$, the orbital parameters e and p can be written as a function of E and L_z, and vice versa. For an equatorial orbit, its orbital frequency is characterized by Ω_r and Ω_ϕ, *i.e.*,

$$\Omega_r = \frac{2\pi}{T_r}, \qquad \Omega_\phi = \frac{\Delta\phi}{T_r}. \tag{13}$$

Here, the radial period T_r and circumstellar shift $\Delta\phi$ can be represented by the simple integral expressions [8, 9]

$$T_r = \int_{r_b}^{r_a}\frac{u^t}{u^r}\mathrm{d}r = \int_0^{2\pi}\frac{\mathrm{d}r}{\mathrm{d}\chi}\frac{u^t}{u^r}\mathrm{d}\chi,$$
$$\Delta\phi = \int_0^{T_r}\frac{u^\phi}{u^t}\mathrm{d}t = \int_0^{2\pi}\frac{\mathrm{d}r}{\mathrm{d}\chi}\frac{u^\phi}{u^r}\mathrm{d}\chi. \tag{14}$$

The number of cycles $\mathcal{N}$ is a quantity that effectively illustrates the difference between Kerr and swirling-Kerr orbits, which requires an accumulated difference of $\pi/2$ in the periastron shift,

$$\mathcal{N}=\frac{\pi/2}{|\Delta\phi_K-\Delta\phi_{sK}|},\tag{15}$$

where the indices K and sK denote the Kerr and swirling-Kerr cases, respectively. The larger the number of cycles $\mathcal{N}$, the smaller the orbital deviations. Figure 1 shows the effects of orbital parameters e, p, and black hole spin a on the periastron shift difference $\Delta\phi_{sK}-\Delta\phi_K$ (left panel), radial period difference $T_{r(sK)}-T_{r(K)}$ (middle panel), and number of cycles $\mathcal{N}$ for different values of the swirling parameter j. The absolute values of these orbital differences, $|\Delta\phi_{sK}-\Delta\phi_K|$ and $|T_{r(sK)}-T_{r(K)}|$, clearly increase with the swirling parameter j, whereas the number of cycles $\mathcal{N}$ decreases. The effects of the parameter j are the opposite of those of the black hole spin parameter a, which may provide a probe to identify the swirling of the universe's background. Moreover, with an increase in the parameter p, the quantities $|\Delta\phi_{sK}-\Delta\phi_K|$ and $|T_{r(sK)}-T_{r(K)}|$ decrease and then increase, whereas the number of cycles $\mathcal{N}$ increases and then decreases. With an increase in the parameter e, the absolute values $|\Delta\phi_{sK}-\Delta\phi_K|$ and $|T_{r(sK)}-T_{r(K)}|$ increase, and the number of cycles $\mathcal{N}$ decreases.

We can now compute the gravitational waveforms caused by the particle's trajectory through the swirling-Kerr spacetime using the kludge waveform generation method. As shown in Ref. [86], adopting Cartesian coordinates $x=r\sin\theta\cos\phi$, $y=r\sin\theta\sin\phi$, $z=r\cos\theta$ and employing the multipolar expansion of metric perturbations can produce the lowest-order term in gravitational waves emitted by an isolated system through the quadrupole formula

$$\bar{h}^{jk}(t,x)=\frac{2}{R}[\ddot{I}^{jk}(t')]_{t'=t-r},\tag{16}$$

where R denotes the luminosity distance from the source to the observer, and $I^{jk}(t')$ is the source's mass quadru-

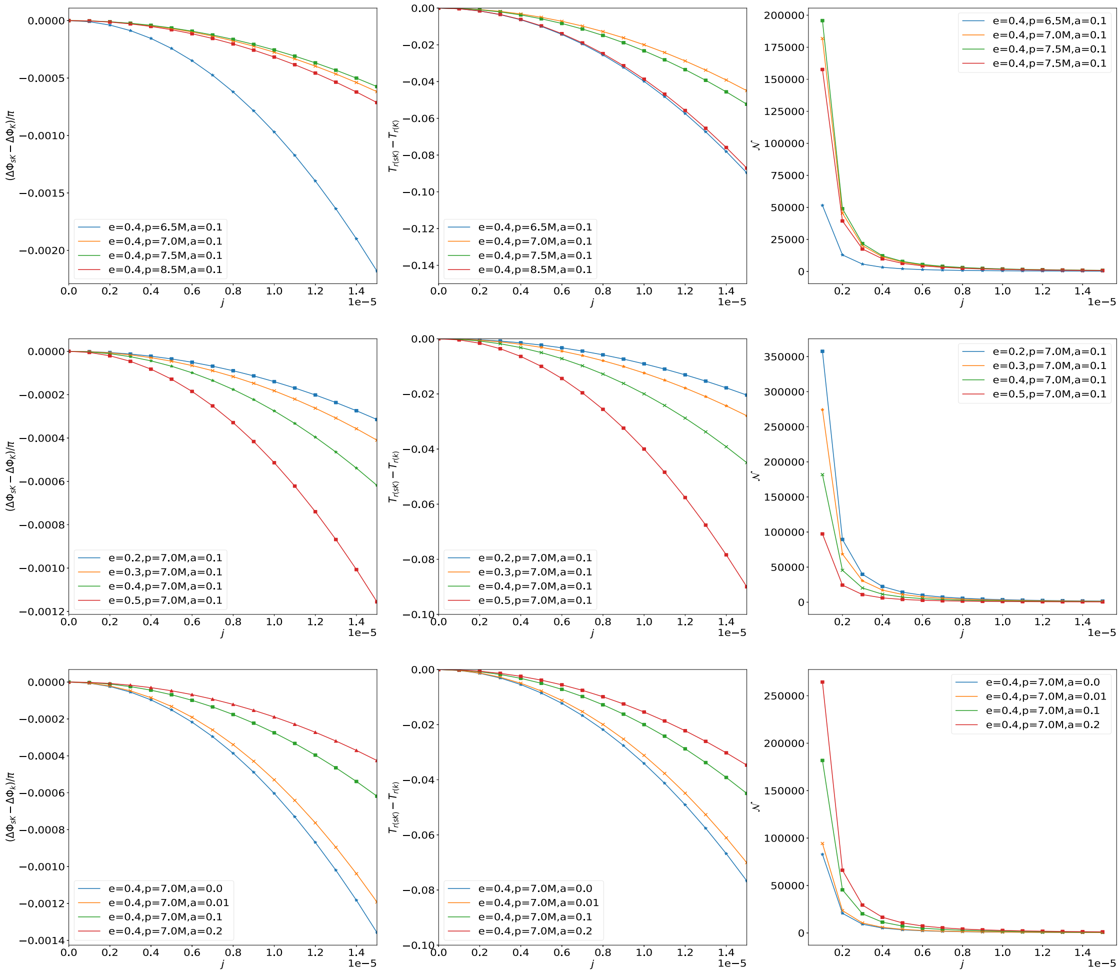

Fig. 1. (color online) Changes in the periastron shift difference $\Delta\phi_{sK}-\Delta\phi_K$ (left panel), radial period difference $T_{r(sK)}-T_{r(K)}$ (middle panel), and number of cycles N (right panel) with the swirling parameter j for different e, p, and a.

pole moment, which has the form

$$I^{jk}(t') = \int x'^j x'^k T^{00}(t', x')\mathrm{d}^3 x'. \tag{17}$$

Following the procedure proposed in Refs. [84, 85], with a transverse-traceless (TT) projection to the previously mentioned expressions and the standard TT gauge, the plus and cross components of the waveform observed at latitude Θ and azimuth Φ can be expressed as

$$\begin{aligned} h_+ = h^{\Theta\Theta} - h^{\Phi\Phi} &= \{\cos^2\Theta[h^{xx}\cos^2\Phi + h^{xy}\sin 2\Phi h^{yy}\sin^2\Phi] \\ &+ h^{zz}\sin^2\Theta - \sin 2\Theta[h^{xz}\cos\Phi + h^{yz}\cos\Phi]\} \\ &- [h^{xx}\sin^2\Phi - h^{xy}\sin 2\Phi + h^{yy}\cos^2\Phi], \\ h_\times = 2h^{\Theta\Phi} &= 2\{\cos\Theta[-\frac{1}{2}h^{xx}\sin 2\Phi + h^{xy}\cos 2\Phi \\ &+ \frac{1}{2}h^{yy}\sin 2\Phi] + \sin\Theta[h^{xz}\sin\Phi - h^{yz}\cos\Phi]\}. \end{aligned} \tag{18}$$

To analyze the distinctions between waveforms in swirling Kerr spacetimes and those predicted from general relativity, we can utilize the overlap function [9]

$$\mathcal{F}(\tilde{h}_1, \tilde{h}_2) = \frac{(\tilde{h}_1 \mid \tilde{h}_2)}{\sqrt{(\tilde{h}_1 \mid \tilde{h}_1)(\tilde{h}_2 \mid \tilde{h}_2)}}, \tag{19}$$

where the quantity marked with "tilde" $\tilde{h}$ denotes the frequency domain signal related to the time domain signal $h(t)$ of a gravitational wave by the Fourier transforms. The inner product $(\tilde{h}_1, \tilde{h}_2)$ is defined by [87–92]

$$(\tilde{h}_1 \mid \tilde{h}_2) = 2\int_0^\infty \frac{\tilde{h}_1^*(f)\tilde{h}_2(f) + \tilde{h}_1(f)\tilde{h}_2^*(f)}{S_n(f)}\mathrm{d}f, \tag{20}$$

where $S_n(f)$ is the signal-to-noise ratio of the detector. The noise spectral density of LISA is [89, 90]

$$S_n(f) = \frac{1}{L^2}\left\{S_x + \left[1 + \left(\frac{0.4\,\mathrm{mHz}}{f}^2\right)\frac{4S_a}{(2\pi f)^4}\right]\right\}. \tag{21}$$

The overlap function $\mathcal{F}(\tilde{h}_1, \tilde{h}_2) = 1$ if the two waveforms are identical, $\mathcal{F}(\tilde{h}_1, \tilde{h}_2) = 0$ if they are totally uncorrelated, and $\mathcal{F}(\tilde{h}_1, \tilde{h}_2) = -1$ if they are perfectly anti-correlated [10]. Therefore, a higher value of the overlap function indicates that it is more difficult to distinguish between the two waveform signals.

III. EFFECTS OF THE SWIRLING PARAMETER ON EMRI GRAVITATIONAL WAVES

Let us now probe the effects of the swirling and black hole spin parameters on EMRI gravitational waves using the numerical kludge method. In our numerical analysis, the primary mass M and secondary mass μ are set as $M = 2\times 10^5\, M_\odot$ (solar mass) and $\mu = 2\, M_\odot$, respectively; thus, the mass ratio $\eta = \mu/M = 10^{-5}$. The observed angular parameters are set to $\Theta = \pi/4$, $\Phi = 0$, and the luminosity distance is $D_L = 5\,\mathrm{Gpc}$. To evaluate the effect of the rotation parameter j on the EMRI gravitational waves, we focus only on the orbital evolutions on the equatorial plane, which are determined by conservative dynamics without explicitly considering radiative reactions.

The initial values of (E, L_z, Q) for the equatorial geodesic orbits in the context of conservative dynamics are given by [85]

$$\begin{aligned} &V_r(E, L_z, Q = 0, r = r_a) = 0, \\ &V_r(E, L_z, Q = 0, r = r_p) = 0, \qquad Q = 0. \end{aligned} \tag{22}$$

Taking the same initial positions and orbital parameters e and p, in Fig. 2, we present the time series of equatorially eccentric motion in the swirling Kerr black hole spacetime for different values of the swirling parameter j over the first 2000 s. For a fixed spin parameter a, we find that j significantly influences the orbit period and phase. As j increases, periods in the r direction decrease, whereas those in the ϕ direction increase. This observation is consistent with the results shown in Fig. 1. With an increase in the spin parameter a, the influence of the swirling parameter j on the orbit decreases. As a increases up to $a = 0.1$, the difference caused by j is almost indistinguishable in both the r and ϕ directions. This means that in the rapidly rotating black hole case, the effects of j can be negligible. This is rational because in this case, the frame dragging of the black hole dominates that of background swirling. These properties of the spacetime parameters on the geodesic orbital trajectories are also shown in Fig. 3.

Based on the geodesic orbits given above, we can generate gravitational waveforms for the plus and cross modes using of the NK method [84, 85], as shown in Figs. 4 and 5, respectively. When $a = 0$ and $a = 0.01$, the parameter j has almost no effect on the gravitational waveforms during the initial 200 s, whereas the impact of j becomes visually apparent after several orbital cycles and causes a phase delay of the gravitational waveforms. When $a = 0.1$, the gravitational waveforms for different j values are visually almost identical in the initial 500 s, and distinct differences appear only after 1800 s. This means that the spin parameter a suppresses the effects of the swirling parameter j on the EMRI gravitational waves. Therefore, we can easily extract information on the swirling parameter j from the EMRI gravitational waves in the slowly rotating black hole case. For the case with a higher spin parameter, to distinguish between the Kerr

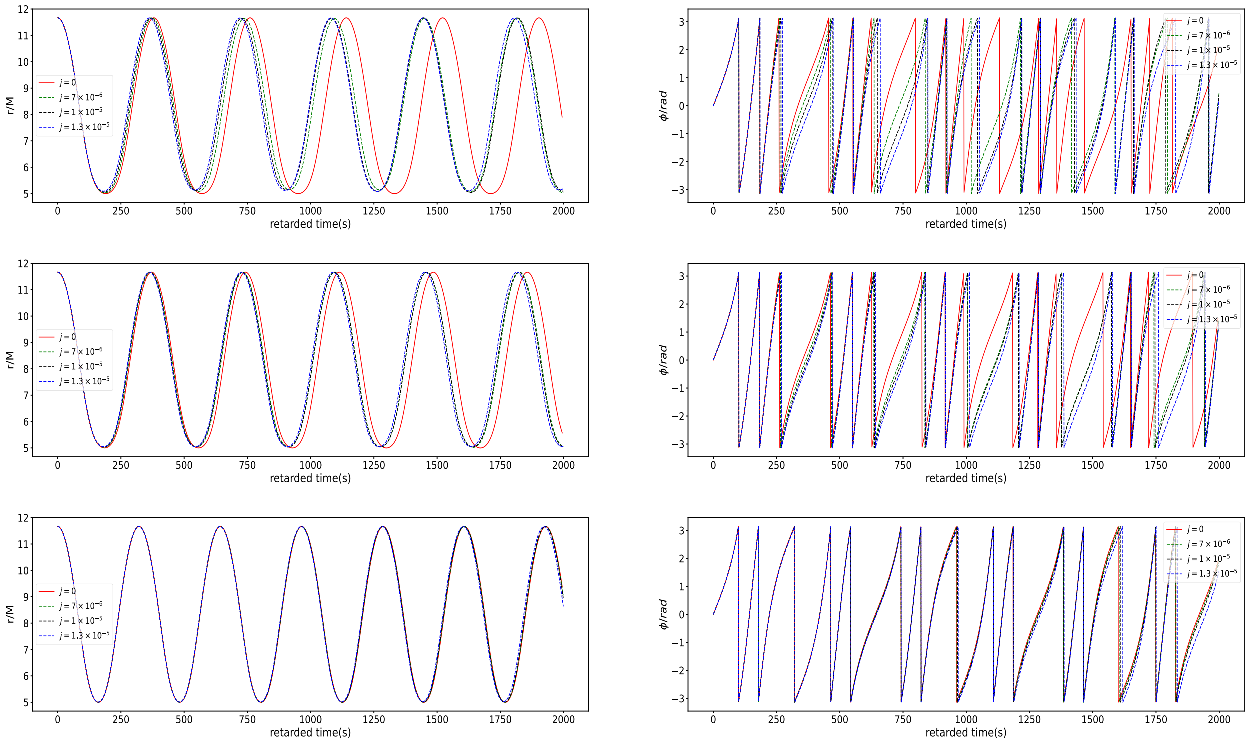

Fig. 2. (color online) Time series of the orbital motion with orbital parameters $e=0.4$ and $p=7.0M$ in the swirling Kerr spacetime for different values of j. The left and right panels correspond to the motion in the r- and ϕ-directions, respectively. The top, middle, and bottom rows denote $a=0.0$, $a=0.01$, and $a=0.1$, respectively.

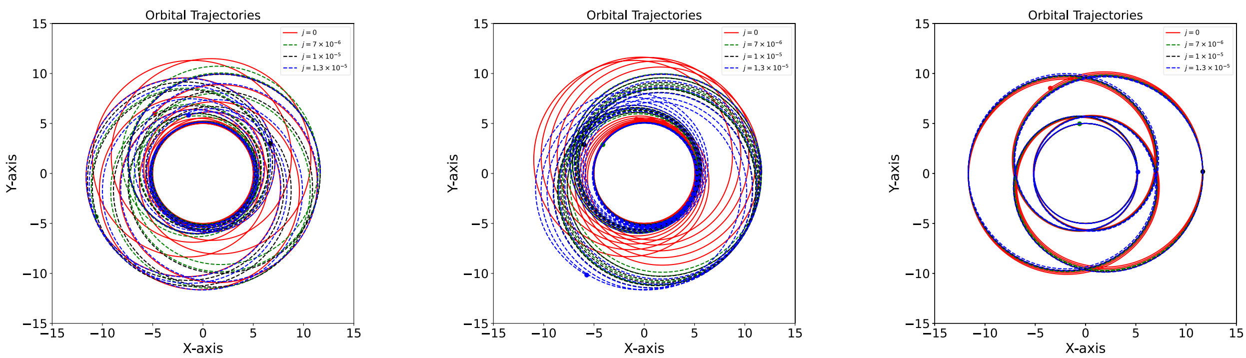

Fig. 3. (color online) Trajectories with orbital parameters $e=0.4$ and $p=7.0M$ in the swirling Kerr spacetime for different values of the swirling parameter j. The left, middle, and right panels correspond to cases with $a=0$, $a=0.01$, and $a=0.1$, respectively.

and swirling-Kerr orbital waveforms, we need a longer retarded time, such that the EMRI gravitational wave can accumulate effects from the swirling parameter j.

As in other cases, the confusion problem is encountered when identifying the signal of the swirling parameter from the EMRI gravitational wave data observed by real detectors. This is mainly because there is potentially a significant overlap between the EMRI gravitational waveforms of Kerr and swirling-Kerr spacetimes, as they share the same orbital frequency. The significant overlap makes it difficult to effectively distinguish between the waveforms in the Kerr and swirling-Kerr cases. As in the previous discussion, we noted that the lager spin parameter leads to a confusion problem where the effects of the swirling parameter j are heavily suppressed. In Fig. 6, we present the orbital deviation between Kerr and swirling-Kerr spacetimes for the parametmeter set $\{e, p, a\}$ = $\{0.4, 7.0, 0.5\}$ for different j and find that the two orbits are almost indistinguishable in this case. In Fig. 7, we also present the overlap function (19) with the retarded time t for different j (left) and with j for the fixed signal length $t=2.6\times10^{6}$ s (right). We find that the overlap value for $j=9\times10^{-7}$ is is still very high even if the retarded time $t=2.6\times10^{6}$ s. This severely hinders our ability to detect the swirling parameter by analyzing EMRI gravitational waveforms. Moreover, Fig.

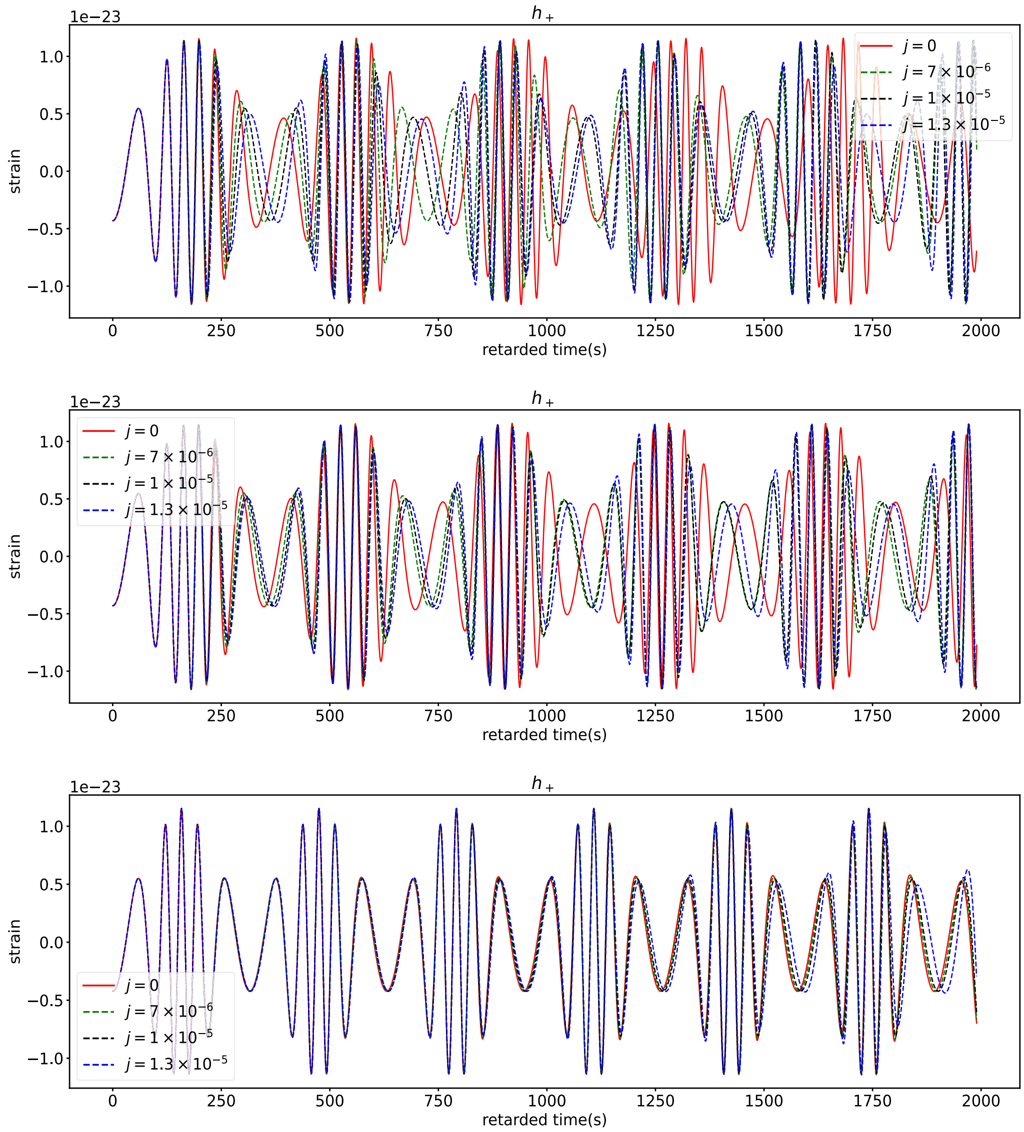

Fig. 4. (color online) Plus component of EMRI waveforms for different values of the swirling parameter j. The top, middle, and bottom rows correspond to the cases with centre black hole's spin $a=0.0$, $a=0.01$, $a=0.1$, respectively. Here, we set the orbital parameters as $e=0.4$ and $p=7.0M$.

7 also shows that the overlap function for the fixed signal length also almost decreases with the swirling parameter j, which is rational because a larger swirling parameter inevitably leads to greater differences between gravitational waveforms in Kerr and swirling-Kerr spacetimes.

Let us discuss the possible confusion of gravitational waves induced by the orbital parameters e and p. As in Ref. [10], one can calibrate the orbital frequency to look for combinations of parameters that might cause waveform confusion

$$\Omega_{ki}(j=0,a_0,M_0,e_0,p_0)=\Omega_{si}(j,a_0,M_0,e_0+\delta e,p_0+\delta p),\quad i=r,\ \phi. \tag{23}$$

Here, δp and δe are two small deviations of the orbital parameters. By solving the above equations, we can obtain deviations δp and δe and further discuss the confusion problem arising from orbital parameters e and p for fixed M, a, and j. In Fig. 8, we present the relationship between the relative variations of the orbital parameters and the black hole parameters j, a, and M by matching the orbital frequency of Kerr and swirling-Kerr black holes. The results reveal that $\delta e/e_0$ increases rapidly and $\delta p/p_0$ decreases rapidly as j increases, which means that changes in the swirling parameter j must adjust the orbital parameters e and p to preserve consistent orbital frequencies. As the black hole spin parameter a increases, $\delta e/e_0$ first decreases and then increases, whereas the change in $\delta p/p_0$ is exactly the opposite of that. This means that ef-

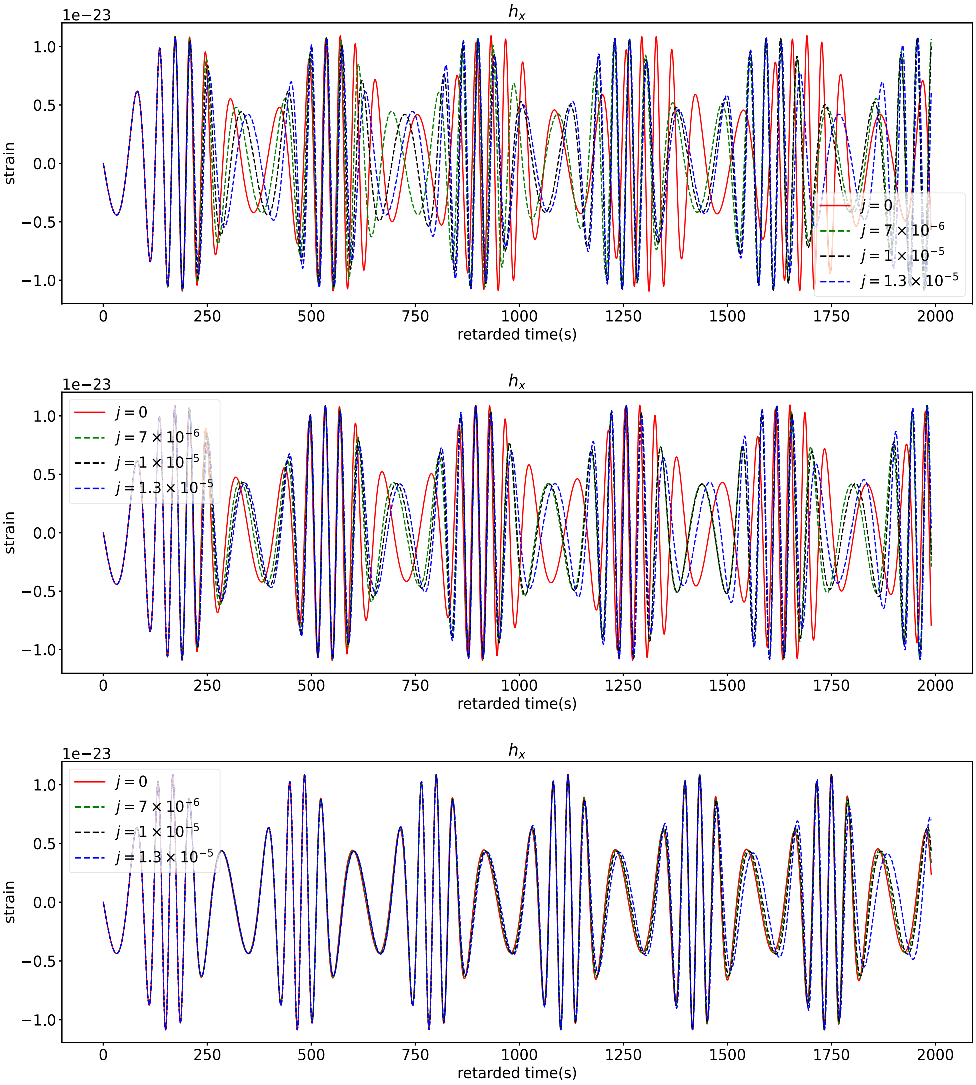

Fig. 5. (color online) Cross component of EMRI waveforms for different values of the swirling parameter j. The top, middle, and bottom rows correspond to the cases with centre black hole's spin $a=0.0$, $a=0.01$, $a=0.1$, respectively. Here, we set the orbital parameters as $e=0.4$ and $p=7.0M$.

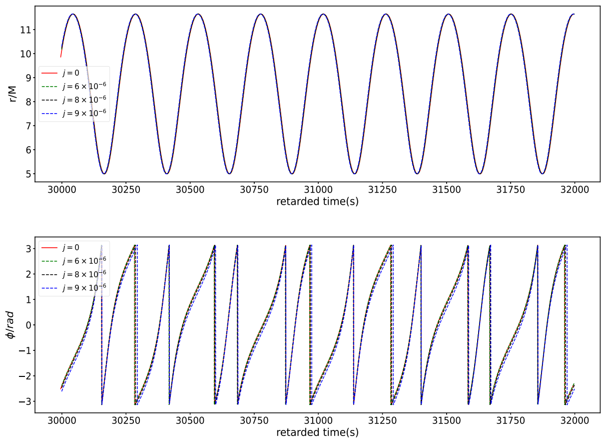

Fig. 6. (color online) Time series in the r and ϕ directions under swirling-Kerr spacetime and Kerr spacetime with the same parameter set $\{e,p,a\}=\{0.4,7.0,0.5\}$ for different swirling parameter j.

fects of the background rotation parameter j on the relative variations $\delta e/e_0$ and $\delta p/p_0$ are distinctly different from those of the black hole spin parameter a. With the increase in the black hole mass M, both $\delta e/e_0$ and $\delta p/p_0$ increase, but $\delta p/p_0$ has a higher rate of change. Furthermore, we find that the change tendencies of $\delta e/e_0$ and $\delta p/p_0$ with the parameter j are similar to those observed with the MOG parameter α in the STVG [47], but the rates are different. Through the above analysis, we find that the confusion problem also exists in the swirling-Kerr case.

IV. SUMMARY

It is important to study gravitational waves in the rotating black hole spacetime deviated from the usual Kerr one. In this study, we investigated the EMRI gravitation-

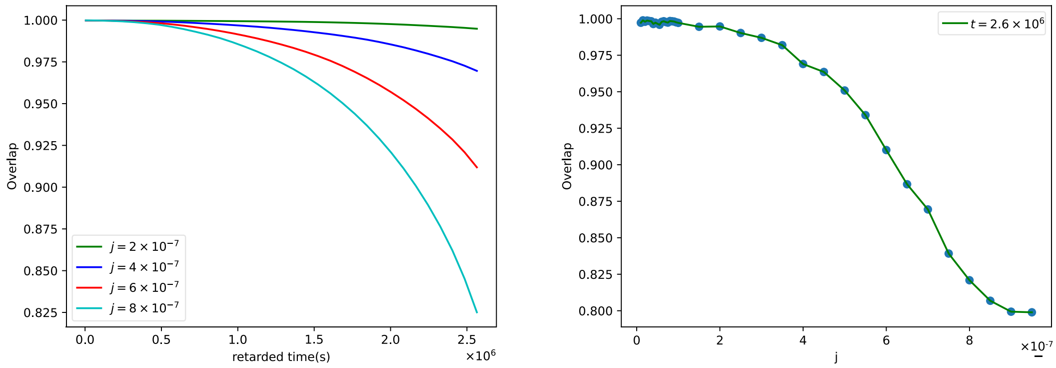

Fig. 7. (color online) Overlap between Kerr and swirling-Kerr spacetimes with retarded time t for different j (left) and with j for the fixed signal length $t = 2\times10^6$ s (right). Here, the parameter set is $\{e,p,a\} = \{0.4,7.0,0.5\}$.

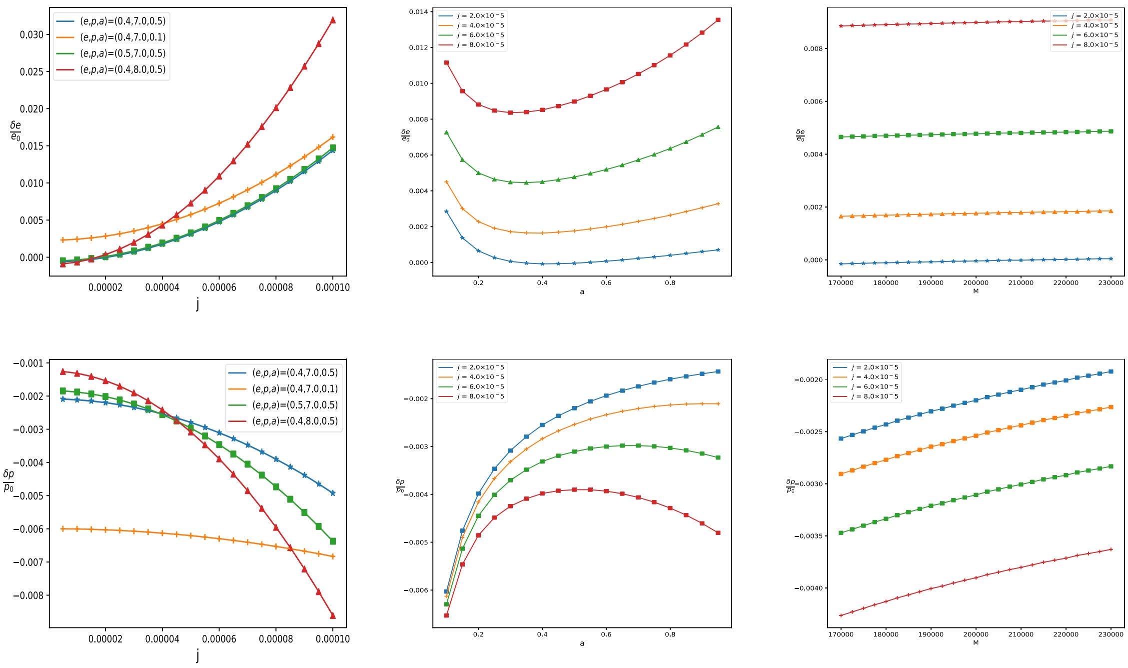

Fig. 8. (color online) Relation between relative varied orbit parameters for different black hole parameters when equating orbital frequencies, *i.e.*, the orbits of $(0,a,M,e_0,p_0)$ and $(j,a,M,e_0+\delta e,p_0+\delta p)$ have the same orbital frequencies. The black hole spin parameter is set to $a = 0.5$ in the left and right panels, and the black hole mass parameter is set to $M = 2\times10^5\ M_\odot$ in the left and middle panels. The orbit parameters are set to $e_0 = 0.4$ and $p_0 = 7.0$ in each panel.

al waves induced by eccentric orbits in the equatorial plane within the framework of the swirling-Kerr black hole spacetimes. The swirling-Kerr black hole is a novel solution of vacuum general relativity and has an extra swirling parameter characterizing the rotation of space-time background. We find that the swirling parameter j enhances the orbital differences between the swirling-Kerr black hole spacetime and the corresponding Kerr black hole spacetime, with effects opposite to those of the black hole spin parameter a. This distinction could serve as a potential probe for identifying the background's swirling. As the parameter p increases, the quantities $|\Delta\phi_{sK}-\Delta\phi_K|$ and $|T_{r(sK)}-T_{r(K)}|$ initially decrease and then increase, whereas the number of cycles $\mathcal{N}$ first increases and then decreases. Contrastingly, as the orbital eccentricity e increases, the absolute values of $|\Delta\phi_{sK}-\Delta\phi_K|$ and $|T_{r(sK)}-T_{r(K)}|$ increase, whereas the number of cycles $\mathcal{N}$ decreases.

For EMRI systems, the presence of the swirling parameter j results in a phase delay in the gravitational waveforms, whereas the black hole spin parameter a suppresses the impact of the swirling parameter j on the EMRI gravitational waves. As a result, extracting information on the swirling parameter j from the EMRI gravitational waves is significantly easier in the case of a slowly rotating black hole spacetime compared to a rapidly rotating black hole. Finally, we also analyze the confusion problem of gravitational waves in the swirling-Kerr black hole spacetime. It is evident that a high black hole spin results in a significant overlap between waveforms for different values of the swirling parameter j. For instance, in the case $a=0.5$, the overlap value for different j remains high even at a retarded time $t=2\times10^6$ s. This significantly hinders our ability to detect the swirling parameter in the rapidly rotating black hole case by analyzing EMRI gravitational waveforms. Additionally, we explore the possible confusion of gravitational waves induced by the orbital parameters e and p. For EMRI gravitational waves with the same orbital frequencies, the allowable relative variations of orbital parameters $\delta e/e_0$ increase rapidly, while $\delta p/p_0$ rapidly as j increases. The change trends of $\delta e/e_0$ and $\delta p/p_0$ with the parameter j are similar to those observed with the MOG parameter α in the STVG theory [47], but the rates are different. As the black hole spin parameter a increases, $\delta e/e_0$ first decreases and then increases, whereas the change in $\delta p/p_0$ is exactly the opposite of that. This means that the effects of the background rotation parameter j on the relative variations $\delta e/e_0$ and $\delta p/p_0$ are distinctly different from those of the black hole spin parameter a. With the increase in the black hole mass M, both $\delta e/e_0$ and $\delta p/p_0$ increase, but $\delta p/p_0$ has a higher rate of change. These results provide further insight into the properties of EMRI gravitational waves and background swirling.

References

[1] B. P. Abbott *et al.* (LIGO Scientific and Virgo Collaborations), Phy. Rev. Lett. **116**, 061102 (2016)
[2] B. P. Abbott *et al.* (LIGO Scientific and Virgo Collaborations), Phy. Rev. Lett. **119**, 161101 (2017)
[3] B. P. Abbott, R. Abbott, T. D. Abbott *et al.*, ApJL. **848**, L12 (2017)
[4] J. R. Gair, L. Barack, T. Creighton *et al*, Class. Quant. Grav. **21**, S1595 (2004), arXiv: gr-qc/0405137
[5] J. R. Gair and K. Glampedakis, Phys. Rev. D **73**, 064037 (2006)
[6] S. A. Hughes, Phys. Rev. D **64**, 064004 (2001)
[7] S. Drasco and S. A. Hughes, Phys. Rev. D **73**, 024027 (2006)
[8] K. Glampedakis and D. Kennefick, Phys. Rev. D **66**, 044002 (2002)
[9] K. Glampedakis and S. Babak, Class. Quant. Grav. **23**, 4167 (2006)
[10] E. Barausse, L. Rezzolla, D. Petroff *et al.*, Phys. Rev. D **75**, 064026 (2007), arXiv: gr-qc/0612123
[11] E. A. Huerta and J. R. Gair, Phys. Rev. D **79**, 084021 (2009), arXiv: 0812.4208
[12] J. R. Gair, E. E. Flanagan, S. Drasco *et al.*, Phys. Rev. D **83**, 044037 (2011)
[13] N. Warburton, S. Akcay, L. Barack *et al.*, Phys. Rev. D **85**, 061501(R) (2012)
[14] C. Moreno-Garrido, E. Mediavilla and J. Buitrago, Mon. Not. R. Astron. Soc. **274**, 115 (1995)
[15] M. D. Hartl and A. Buonanno,Phys. Rev. D **71**, 024027 (2005)
[16] K. Glampedakis, Class. Quant. Grav. **22**, S605 (2005), arXiv: gr-qc/0509024
[17] W. B. Han, Phys. Rev. D **82**, 084013 (2010)
[18] W. B. Han, Int. J. Mod. Phys. D **23**(07), 1450064 (2014)
[19] W. B. Han, Class. Quantum Grav. **33**, 065009 (2016), arXiv: 1609.06817
[20] C. P. L. Berry, S. A. Hughes, C. F. Sopuerta *et al.*, Bull. Am. Astron. Soc. **51**, 42 (2019), arXiv: 1903.03686
[21] A. Torres-Orjuela, S. J. Huang, Z. C. Liang *et al.*, Sci. China Phys. Mech. Astron. **67**(5), 259511 (2024), arXiv: 2307.16628
[22] P. Amaro-Seoane *et al.* (LISA Collaboration), arXiv: 1702.00786
[23] K. Danzmann, Class. Quant. Grav. **14**, 1399 (1997)
[24] W. Hu and Y. Wu, Natl. Sci. Rev. **4**, 685 (2017)
[25] Y. Gong, J. Luo, and B. Wang, Nature Astron. **5**, 881 (2021), arXiv: 2109.07442
[26] J. Luo *et al.* (TianQin Collaboration), Class. Quant. Grav. **33**, 035010 (2016), arXiv: 1512.02076
[27] E. Barausse, E. Berti, T. Hertog *et al.*, Gen. Rel. Grav. **52**(8), 81 (2020), arXiv: 2001.09793
[28] P. A. Seoane *et al*, (LISA Collaboration), Living Rev. Rel. **26**(1), 2 (2023), arXiv: 2203.06016
[29] K. G. Arun *et al.* (LISA Collaboration), Living Rev. Rel. **25**(1), 4 (2022), arXiv: 2205.01597
[30] N. Karnesis, N. Stergioulas, G. Pappas *et al.*, Int. J. Mod. Phys. D **33**, 2450027 (2024), arXiv: 2209.04358
[31] J. R. Gair, M. Vallisneri, S. L. Larson *et al.*, Living Rev. Rel. **16**, 7 (2013), arXiv: 1212.5575v2
[32] G. A. Piovano, A. Maselli, and P. Pani, Phys. Lett. B **811**, 135860 (2020), arXiv: 2003.08448
[33] S. Datta and S. Bose, Phys. Rev. D **99**, 084001 (2019), arXiv: 1902.01723
[34] A. G. Shah, J. L. Friedman, and T. S. Keidl, Phys. Rev. D **86**, 084059 (2012), arXiv: 1207.5595
[35] S. Xin, W. Han, and S. Yang, Phys. Rev. D **100**, 084055 (2019), arXiv: 1812.04185
[36] S. Kumar, arXiv: 2410.08544
[37] A. Chowdhuri, A. Bhattacharyya, and S. Kumar, JCAP **04**, 001 (2024), arXiv: 2311.05983
[38] S. Kumar, R. K. Singh, A. Chowdhuri *et al.*, JCAP **10**, 047 (2024), arXiv: 2405.18508
[39] M. Rahman, S. Kumar, and A. Bhattacharyya, JCAP **01**, 035 (2024), arXiv: 2306.14971
[40] S. Kumar, arXiv: 2412.11847
[41] M. Rahman, S. Kumar, and A. Bhattacharyya, JCAP **01**, 046 (2023), arXiv: 2212.01404
[42] N. V. Krishnendu and S. Chakraborty, Phys. Rev. D **109**(12), 124047 (2024), arXiv: 2402.15336
[43] S. Mukherjee and S. Chakraborty, Class. Quant. Grav. **40**(14), 145013 (2023), arXiv: 2212.07018
[44] R. Ghosh, K. Chakravarti, JCAP **04**, 037 (2025), arXiv: 2406.02454
[45] E. Berti, A. Buonanno, and C. M. Will, Class. Quant. Grav. **22**, S943 (2005), arXiv: gr-qc/0504017
[46] N. Yunes, P. Pani, and V. Cardoso, Phys. Rev. D **85**, 102003 (2012), arXiv: 1112.3351
[47] X. Qiao, Z. Xia, Q. Pan *et al.*, JCAP **03**, 006 (2025), arXiv: 2408.10022

[48] C. F. Sopuerta and N. Yunes, Phys. Rev. D **80**, 064006 (2009), arXiv: 0904.4501
[49] P. Pani, V. Cardoso, and L. Gualtieri, Phys. Rev. D **83**, 104048 (2011), arXiv: 1104.1183
[50] P. Canizares, J. R. Gair, and C. F. Sopuerta, Phys. Rev. D **86**, 044010 (2012), arXiv: 1205.1253
[51] S. Yang, Y. P. Zhang, T. Zhu *et al.*, Chin. Phys. **49**, 115107 (2025), arXiv: 2412.04302
[52] T. Zi and S. Kumar, Eur. Phys. J. C **85**, 592 (2025), arXiv: 2409.17765
[53] G. Fu, Y. Liu, B. Wang *et al.*, Phys. Rev. D **111**, 084066 (2025), arXiv: 2409.08138
[54] V. De Falco, E. Battista, D. Usseglio *et al.*, Eur. Phys. J. C **84**(2), 137 (2024), arXiv: 2401.13374
[55] V. De Falco and E. Battista, Phys. Rev. D **108**(6), 064032 (2023), arXiv: 2309.00319
[56] E. Battista, V. De Falco, and D. Usseglio, Eur. Phys. J. C **83**(2), 112 (2023), arXiv: 2301.08954
[57] E. Battista and V. De Falco, Eur. Phys. J. C **82**(9), 782 (2022), arXiv: 2208.09839
[58] E. Battista and V. De Falco, Eur. Phys. J. C **82**(7), 628 (2022), arXiv: 2206.12907
[59] E. Battista and V. De Falco, Phys. Rev. D **104**(8), 084067 (2021), arXiv: 2109.01384
[60] C. F. B. Macedo, P. Pani, V. Cardoso *et al.*, Astrophys. J. **774**, 48 (2013), arXiv: 1302.2646
[61] O. A. Hannuksela, K. C. Y. Ng, and T. G. F. Li, Phys. Rev. D **102**, 103022 (2020), arXiv: 1906.11845
[62] N. Dai, Y. G. Gong, Y. Zhao *et al.*,Phys. Rev. D **110**, 084080 (2024), arXiv: 2301.05088
[63] A. Maselli, N. Franchini, L. Gualtieri *et al.*, Phys. Rev. Lett. **125**, 141101 (2020), arXiv: 2004.11895
[64] A. Maselli, N. Franchini, L. Gualtieri *et al.*, Nature Astron. **6**, 464 (2022), arXiv: 2106.11325
[65] H. Guo, Y. Liu, C. Zhang *et al.*, Phys. Rev. D **106**, 024047 (2022), arXiv: 2201.10748
[66] Y. P. Zhang, Y. B. Zeng, Y. Q. Wang *et al.*, arXiv: 2108.13170
[67] S. Barsanti, N. Franchini, L. Gualtieri *et al.*, Phys. Rev. D **106**, 044029 (2022), arXiv: 2203.05003
[68] C. Zhang, Y. Gong, D. Liang *et al.*, JCAP **06**, 054 (2023), arXiv: 2210.11121
[69] H. Guo, C. Zhang, Y. Liu *et al.*, Chin. Phys. C **48**, 095103 (2024), arXiv: 2305.00652
[70] S. Barsanti, A. Maselli, T. P. Sotiriou *et al.*, Phys. Rev. Lett. **131**, 051401 (2023), arXiv: 2212.03888
[71] T. Zi, Z. Zhou, H. T. Wang *et al.*, Phys. Rev. D **107**, 023005 (2023), arXiv: 2205.00425
[72] D. Liang, R. Xu, Z. F. Mai *et al.*, Phys. Rev. D **107**, 044053 (2023), arXiv: 2212.09346
[73] C. L. MacLeod and C. J. Hogan, Phys. Rev. D **77**, 043512 (2008)
[74] M. Astorino, R. Martelli, and A. Viganò, Phys.Rev.D **106**, 064014 (2022)
[75] F. J. Ernst, Phys. Rev. **167**, 1175 (1968)
[76] F. J. Ernst, Phys. Rev. **168**, 1415 (1968)
[77] D. Cao, L. Zhang, S. Chen *et al.*, Eur. Phys. J. C **85**, 28 (2025), arXiv: 2410.03214
[78] R. Capobianco, B. Hartmann, and J. Kunz, Phys. Rev. D **109**, 064042 (2024), arXiv: 2312.17347
[79] Z. S. Moreira, C. A. R. Herdeiro, and L. C. B. Crispino, Phys. Rev. D **109**, 104020 (2024), arXiv: 2401.05658
[80] C. Chen, Q. Pan, and J. Jing, Eur. Phys. J. C **84**(10), 1040 (2024), arXiv: 2402.02789
[81] K. Gjorgjieski and R. Capobianco, Eur. Phys. J. C **85**, 597 (2025), arXiv: 2405.16758
[82] J. Barrientos, A. Cisterna, I. Kolář *et al.*, Eur. Phys. J. C **84**, 724 (2024), arXiv: 2401.02924
[83] J. Barrientos, A. Cisterna, M. Hassaine *et al.*, Phys. Lett. B **860**, 139214 (2025), arXiv: 2409.12336
[84] S. Babak, H. Fang, J. R. Gair *et al.*, Phys. Rev. D **75**, 024005 (2007)
[85] A. J. K. Chua, C. J. Moore, and J. R. Gair, Phys. Rev. D **96**, 044005 (2017)
[86] K. S. Thorne, Rev. Mod. Phys. **52**, 299 (1980)
[87] L. Barack and C. Cutler, Phys. Rev. D **69**, 082005 (2004)
[88] L. S. Finn, Phys. Rev. D **46**, 5236 (1992)
[89] T. Robson, N. Cornish, and C. Liu, Class. Quant. Grav. **36**, 105011 (2019), arXiv: 1803.01944
[90] S. Babak, M. Hewitson, and A. Petiteau, arXiv: 2108.01167
[91] C. Cutler and E. Flanagan, Phys. Rev. D **49**, 2658 (1994)
[92] R. Balasubramanian, B. S. Sathyaprakash, and S. V. Dhurandhar, Phys. Rev. D **53**, 3033 (1996)